Astronomy & Astrophysics manuscript no. output
March 15, 2021

Pulsar Scintillation Studies with LOFAR. I. the census

Ziwei Wu[1], *[1], and *[1]

[1] Fakultät für Physik, Universität Bielefeld, Postfach 100131, 33501 Bielefeld, Germany
e-mail:
[2] Max-Planck-Institut für Radioastronomie, Auf dem Hügel 69, 53121 Bonn, Germany

Received **; accepted **

ABSTRACT

Interstellar scintillation of pulsar emission can both be used as a probe of the ionised interstellar medium (IISM) and cause corruptions in pulsar timing experiments. Specially, the relatively recent discovery of scintillation arcs provides wealthy information about the underlying scattering screen and can be used to measure the time-variable time delay of pulse signal directly which may led to improve timing precision significantly. In this work, we report that 15 nearby pulsars show interstellar scintillation effect clearly with the LOw Frequency ARray. The numerous scintles even with narrow band allow through and self-consistent statistical analyses of scintillation frequency scaling laws without the influence coming from refractive scintillation. Our results show that the properties of the IISM in the line of sight of most of pulsars are consistent with the prediction of Kolmogorov spectrum or Gaussian spectrum. The resolved scintillation arcs detected from 9 pulsars allow one to determine the placement and the spatial scale (AU size) of the underlying phase-changing scattering screen. Moreover, the phenomenon of pulse nulling and scintillation are observed simultaneously, but nevertheless, scintillation bandwidth seems still measurable accurately.

Key words. interstellar medium – pulsar scintillation – DM

1. Introduction

The pulsar signal is constantly perturbed by refractive index fluctuation in an ionized interstellar medium (IISM), generating an random phase variation of each incoming ray. The interference between these essentially uncorrelated scattered rays and the relative motion of the pulsar, scattering material in the line of sight (LOS) and the observer results in a modulation of the pulse intensity as a function of frequency, time and position of the observer which is well-known as interstellar scintillation (ISS). The two sub-fields of ISS are diffractive ISS (DISS) caused by the small-spatial-scale density fluctuations ($10^6 - 10^8$ m) and refractive ISS (RISS) resulted from large-spatial-scale density inhomogeneities ($10^{10} - 10^{12}$ m) in the IISM, which remains distinct in the strong scattering region where generous scattered rays interference with one another to form an interference pattern on the observer plane (multi-path propagation). Good reviews of ISS theory and phenomena may found in Rickett (1990) and Narayan (1992).

Scintles, i.e. enhanced pulse intensity variations on relatively short time scale and small frequency bandwidth, are identified in the ISS primary production that is the dynamic spectra which is a two-dimensional matrix of the pulse intensity as a function of time (t) and frequency (ν). With scintillation parameters obtained from dynamic spectrum, one could study the density turbulence in the IISM (Cordes et al. 1985; Spangler & Gwinn 1990), local bubble (Bhat et al. 1998), the restriction on the pulsar proper motion (Cordes 1986; Gupta 1995), the properties of binary system (Coles et al. 2005; Rickett et al. 2014), refractive scintillation (Bhat et al. 1999a) and model the IISM based on the annual variation of scintillation velocity (Reardon et al. 2019), etc.

Two decades ago, scintillation arcs have been confirmed in secondary spectra that are the power spectrum of the dynamic spectra (Stinebring et al. 2001). These scintillation arcs probing the IISM structure, which are frequently observed 'criss-cross' sloping bands, result from interference between rays in a central core and scattered rays from an extended scattering disc (Walker et al. 2004; Cordes et al. 2006). Up to now, the scintillation arcs already reveal its capabilities (e.g. Trang & Rickett 2007; Walker et al. 2008; Brisken et al. 2010; Pen & Levin 2014; Main et al. 2020; Reardon et al. 2020). Yao et al. (2021) first identified the strong correlation between supernova shell and the scattering screen that causes the ISS and reported the first evidence for three-dimensional alignment between the spin and velocity vectors as well.

High-precision pulsar timing experiments, such as pulsar timing arrays (PTA), are promising method of detecting and characterizing low-frequency gravitational waves (e.g. Verbiest et al. 2016; Verbiest & Shaifullah 2018). PTA experiments currently rely on stable millisecond pulsars with low dispersion measure at high frequencies (mostly at 1.4 GHz) to minimize propagation effects on pulsar timing precision. The two branches of propagation effects that could affect the pulsar timing precision are dispersion and scattering. Dispersion is well-studied and its effect on pulsar timing can be eliminated completely and automatically. Scintillation and pulse broadening that are related (Cordes & Rickett 1998) are the most important effects. However, at high observing frequencies, nearby pulsars could be in weak scintillation region causing small number of scintles in the dynamic spectra and have relatively small pulse broadening delay time. A possible way to mitigate the propagation effect on PTA at high frequencies could be monitor pulsars at low frequencies, to correct the high frequency pulsar data. There are four ways from scintillation side to measure the scattering time delays: the relationship between scintillation bandwidth and pulse

delay (Levin et al. 2016), power distribution of the secondary spectra (Hemberger & Stinebring 2008; Main et al. 2020), a direct measurement from pulse profile (e.g. Krishnakumar et al. 2019) and holographic techniques (Walker et al. 2008; Pen & Levin 2014) which may led to improve the timing precision significantly.

In this work, we present the first census of scintillating pulsars with the LOw Frequency ARray (LOFAR), and the optimal frequency and time resolution for long-term monitoring as the scattering delay is time variable. This work has been organized in the following manner: in Section 2 we describe our observations and data processing; in Section 3 we show the analysis and results. section 4 is our conclusion.

2. Observations and data processing

2.1. Observations

Our analysis is based on data from five international LOFAR stations (van Haarlem et al. 2013), namely the stations in Effelsberg (DE601), Tautenburg (DE603) and Potsdam-Bornim (DE604), Norderstedt (DE609) and nançay (FR606) in stand-alone mode, and LOFAR core from time to time in the frequency range 120-180 MHz (see Table 1). Our pulsar processing pipeline was based on DSPSR2 (van Straten & Bailes 2011) with different setting of frequency and time resolution (Table.1) in order to resolve scintles. Subsequently, observations were written out in PSRCHIVE3 format (Hotan et al. 2004).

2.2. Data processing

2.2.1. Radio-frequency interference (RFI)

The RFI cleaning program iterative_cleaner[1] is a modification of the RFI cleaner 'SURGICAL' included in the COASTGUARD python package (Lazarus et al. 2016). Two major changes were made: First, the iterative_cleaner uses an iterative approach for the template profile. which works well particularly when the pulsar signal is annihilated by strong RFI. Second, the de-trending algorithm for correcting slow changes in the residuals was removed.

2.2.2. Scintillation parameters

After polarisation scrunch to total intensity with *pam*, we create the initial dynamic spectrum with *dynamic_spectra* or *psrflux* command. Trends in the frequency direction as a result of spectral index of the pulsar and the sensitivity of LOFAR as well as the time direction due to elevation dependent sensitivity have to removed from the dynamic spectrum. The mean value of the dynamic spectrum has to be subtracted from the dynamic spectrum as well.

Using the dynamic spectrum, one can estimate the diffractive scintillation bandwidth $\Delta\nu_{\rm d}$, diffractive scintillation time-scale $\tau_{\rm d}$ by computing a two-dimensional autocovariance function (2D ACF) of the dynamic spectrum. To calculate 2D ACF, we pad each dynamic spectra with an equal length of zeroes in frequency and time dimensions, perform a 2D fast Fourier transform (FFT), take the squared magnitude of the result, and perform an inverse 2D FFT, following Reardon et al. (2019). Since the center of 2D ACF is often visible as a noise bridge, it is replaced by the mean value of nearby points. Then the 2D ACF is normalized.

[1] https://github.com/larskuenkel/iterative_cleaner

In this work, the title of 2D ACF does not present. Moreover, there is no correlation of the physics between $\Delta\nu_{\rm d}$ and $\tau_{\rm d}$. Thus, after the 2D ACF is obtained for each segment, we make use of 1-dimensional cuts of the 2D ACF along frequency lags $\nu = 0$ and time lags $\tau = 0$ axes to estimate $\Delta\nu_{\rm d}$ and $\tau_{\rm d}$ with Eq.1:

$$\begin{aligned} \mathrm{ACF}(\nu = 0, \tau) &= \exp(-\mathrm{a} * \tau^2) \\ \mathrm{ACF}(\nu, \tau = 0) &= \exp(-\mathrm{b} * \nu) \end{aligned} \tag{1}$$

Then the scintillation parameters are given by

$$\begin{aligned} \tau_d &= \sqrt{\frac{1}{a}} \\ \Delta\nu_d &= \frac{\ln 2}{\mathrm{b}} \end{aligned} \tag{2}$$

The uncertainty of the individual points of slice 2D ACF is given by Eq.1 of Bhat et al. (1999b). Due to the limited resolutions of the dynamic spectrum in frequency and time, the scintles appear bigger than they really are. This effect in both these parameters can be corrected for by subtracting the resolution from the parameters quadratically (Bhat et al. 1999b):

$$\begin{aligned} \Delta\nu_d &= \sqrt{\Delta\nu_d^2 - \Delta f^2} \\ \tau_d &= \sqrt{\tau_d^2 - \Delta t^2} \end{aligned} \tag{3}$$

where, Δf and Δt are the frequency and time resolutions (in Tab.1), respectively. The uncertainty of the scintillation parameters consists of the uncertainty coming from the fitting procedure and the statistical error $\sigma_{\rm est}$ due to the finite number of scintles (see Eq. 4). Ultimately, these two uncertainty sources are added quadratically to get the error.

$$\sigma_{\rm est} = (\mathrm{f_d} * \frac{\mathrm{BW_{dyn}T_{dyn}}}{\Delta\nu_{\rm d}\tau_{\rm d}})^{-0.5}. \tag{4}$$

Here, $\mathrm{BW_{dyn}}$ and $\mathrm{T_{dyn}}$ are the frequency band and length of interested dynamic spectrum, respectively. f_d is the filling factor. For J0953+0755, $\sigma_{\rm est}$ is about 17%. In contrary, $\sigma_{\rm est}$ mostly can be smaller than <1% for other pulsars at LOFAR frequency range even with 10 MHz frequency band while testing the properties of IISM spectra (sec.3.1.2).

To compute the secondary spectra, we apply a Hamming window function to the outer 10% of each dynamic spectrum. After this, we form the secondary spectrum using a 2D discrete Fourier transform, taking its squared magnitude, shifting it, and then converting the relative power levels into a decibel scale. The arc curvature was obtained based on the Hough-Transform (Bhat et al. 2016).

3. Analysis and results

The interstellar features, i.e. scintles, can be observed from 15 pulsars at LOFAR frequencies (Fig.1). The size of scintles vary from pulsar to pulsar in both frequency and time domains. In particular, even with 0.1 MHz narrow frequency band of J0332+5434, J0826+2637 and J2219+4754, the presence of "criss-cross" structure from multi pulsars (for example, J0837+0610 and J0953+0755) identifies the presence of scintillation arc, which proves the high feasibility of ISS studies through pulsars with LOFAR as well.

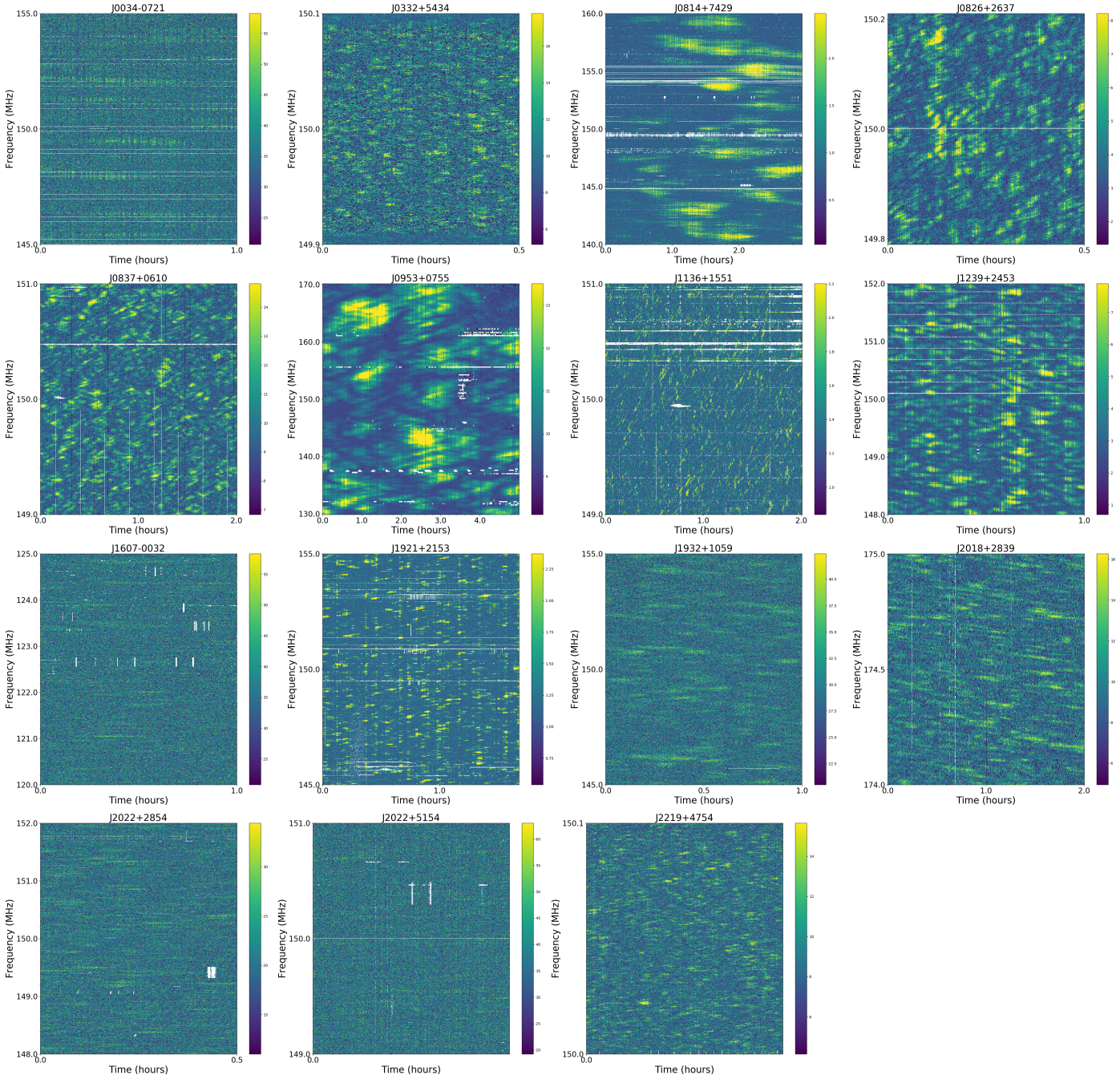

Fig. 1: Dynamic spectra of 15 scintillating pulsars with LOFRA. The white patches were removed because of radio-frequency interference. The colour scale indicates the pulse SNR ranging from blue (no signal) to yellow(high-SNR), which is heavily modulated due to diffraction in the interstellar medium. The high-SNR "islands" are commonly referred to as scintles and provide information on the turbulent interstellar plasma.

The parameter of scattering strength u (Eq.5), defined as the ratio of the Fresnel scale to the DISS scale[2] $s_{\rm d}$ (Rickett 1990), is given by (in terms of $\Delta\nu_{\rm d}$):

$$u \approx (\frac{2\nu}{\Delta\nu_d})^{0.5} \tag{5}$$

The observed values of u from 15 pulsars are given in column 10 of Tab.1 These pulsars are both in strong scattering region ($u > 1$), even the closest pulsar J0953+0755 in our scintillation pulsar list, identifying the multi-path propagation effect.

We estimate the RISS time-scale $t_{\rm r}$ as follow (Rickett 1990):

$$t_{\rm r} \approx \frac{2\nu}{\Delta\nu_d}\tau_{\rm d}. \tag{6}$$

The observed values of $t_{\rm r}$ are showed in column 11 of Tab.1. The $t_{\rm r}$ is longer at lower frequency band ($t_{\rm r} \propto \nu^{-2.2}$ under the assumption of kolmogorov spectra). The observing length of our data set is always shorter than $t_{\rm r}$, proclaiming the modulation from RISS on DISS measurements. We note that the $\tau_{\rm d}$ strongly depends

[2]The spatial scale of the diffractive scattering, $s_{\rm d}$ is defined as the transverse separation where incident waves have a 1 radian rms difference in phase.

Table 1: The properties of the 15 scintillating pulsars from LOFAR

Name (PSRs J)	Station	Date (YY-MM-DD)	Length (hours)	Δf (kHz)	Δt (sec)	$\Delta\nu_d^*$ (kHz)	τ_d^* (min)	α	u	t_r (Day)
0034-0721	FR606	2020-10-01	1	5	10	82.65 ± 0.39	-	X	60	-
0332+5434	FR606	2020-12-08	0.5	0.3	10	0.77 ± 0.00	0.76 ± 0.00	X	624	206
0814+7429	DE604	2017-04-29	3	5	10	357.81 ± 15.79	23.11 ± 1.02	X	30	13
0826+2637	Core	2019-12-03	0.5	1	5	5.15 ± 0.01	0.65 ± 0.00	X	241	26
0837+0610	DE601	2020-01-19	2	5	10	9.42 ± 0.03	1.82 ± 0.01	X	178	40
0953+0755	DE601	2016-01-04	5	195	60	894.52 ± 55.37	17.89 ± 1.08	X	17	4
1136+1551	DE601	2015-04-10	2	5	10	6.58 ± 0.01	0.41 ± 0.00	X	214	13
1239+2453	FR606	2020-05-20	1	5	10	33.95 ± 0.25	2.21 ± 0.02	X	94	14
1607-0032	FR606	2020-09-08	1	1.25	10	11.70 ± 0.09	7.69 ± 0.06	X	160	137
1921+2153	DE609	2018-08-26	1.7	5	10	21.39 ± 0.07	1.15 ± 0.00	X	118	11
1932+1059	FR606	2020-12-30	1	5	10	52.08 ± 0.64	3.12 ± 0.15	X	76	13
2018+2839	DE603	2019-12-27	2	5	10	-	-	-	-	-
	FR606	2020-12-15	1	0.3	10	1.43 ± 0.01	4.34 ± 0.02	X	458	632
2022+2854	Core	2019-12-03	0.5	1	5	5.08 ± 0.02	2.36 ± 0.01	X	243	97
2022+5154	Core	2019-12-03	0.5	1	5	4.51 ± 0.02	-	X	258	-
2219+4754	Core	2020-01-15	0.5	0.08	5	0.20 ± 0.00	0.55 ± 0.00	X	1225	572

*scintillation bandwdith $\Delta\nu_d$ and scintillation time-scale τ_d in 120-180 MHz, except J1136+1551, J0332+5434 (140-160 MHz) and J2219+4757 (145-155 MHz).

on the earth motion ($\leqslant$ 30 km/s) particularly for a sub-class pulsars with slow transverse velocity leading to variation of the t_r at different epochs. Our discussions relying on single observation are under the assumption of negligible influence resulting from RISS as the observing length of hours is shorter than t_r of days.

3.1. Turbulence Characteristics of the IISM

Within the spatial range between inner and outer scales of turbulence called inertial sub-range scales, the electron density fluctuations are well-known Kolmogorov spectrum (pure energy cascade). The inner scale is constrained by ~100 km (Spangler & Gwinn 1990; Rickett et al. 2009), and the outer scale size is comparable with ~ 100 pc (Armstrong et al. 1995; Xu & Zhang 2017) or 1-20 pc (Rickett et al. 2009). It is now well accepted that the underlying scattering screen could be anisotropic (Coles et al. 2005; Brisken et al. 2010). However, the knowledge of those IISM is still poor understanding.

3.1.1. scintillation bandwidth vs DM

To study the dependence of ISS and DM we have scintillation bandwidth as a function of DM (Fig. 2). The thin screen theory predicts that

$$\Delta\nu_{\rm d} \sim DM^{-2.2}\nu^4 \quad (7)$$

Wolszczan (1977) found that the this two parameters conform to the theoretical slope of -2 remarkably well. However, Balasubramanian & Krishnamohan (1985) found that there are three pulsars (PSR B0628-28, B0833-45 and B1933+16) that seem to deviate significantly from the general trend of the other points. It is known that the Gum nebula causes excessive scattering in the case of Vela pulsar (e.g. Backer 1974).

The variation of $\Delta\nu_{\rm d}$ with DM shows a correlation, however, which is steeper than the 2.2 slope for a Kolmogorov spectrum. There are several arguments to interpret this discrepancy: large scale variations in mean electron density (Hall 1980) and the variations of level of turbulence $C_{\rm n^2}$ (Rickett 1977; Cordes et al. 1985). We note that the measurements of scintillation bandwidth do not eliminate the effect from RISS, the number of scintillating pulsar also needs to be increased to have more precise constrains.

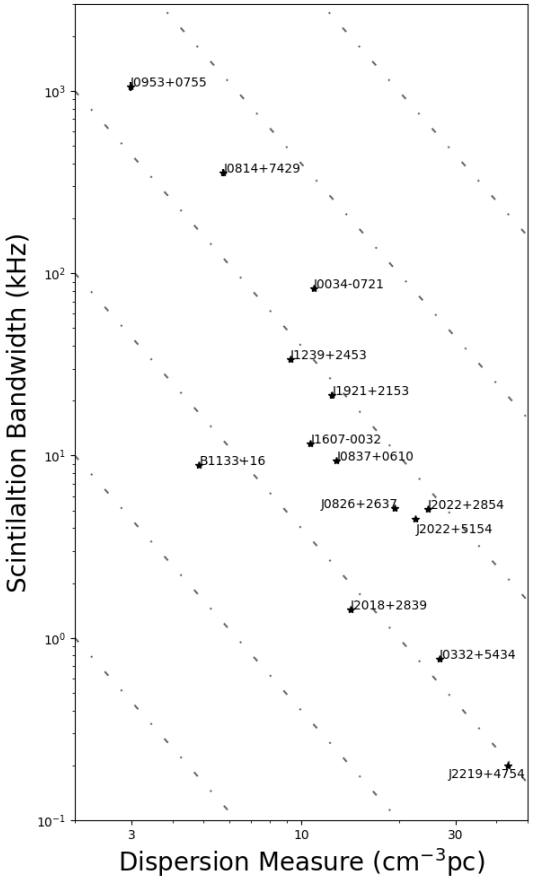

Fig. 2: Scintillation bandwidth Vs DM. The filled circles indicate the pulsars with high galactic latitude (b > 30) and low latitude sources (b <10). The loosely dashdootted lines illustrate ν^{-2} dependence.

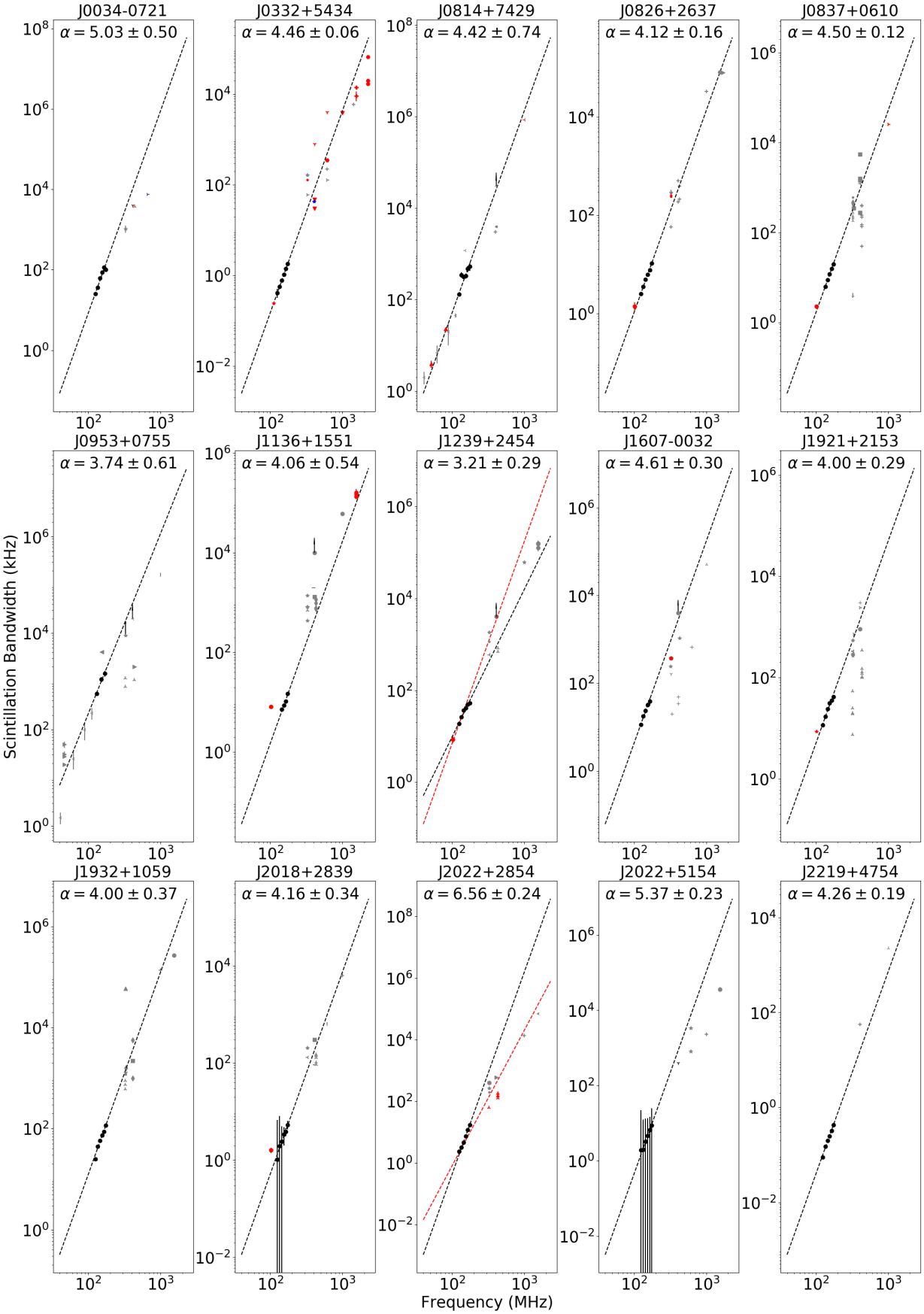

Fig. 3: The scintillation bandwidth VS observing frequency.

3.1.2. Frequency dependence of scintillation bandwidth

The high sensitivity and the fact that even a narrow frequency band can achieve numerous scintles (Fig.1), allow through and self-consistent statistical analyses of scintillation frequency scaling laws, particularly, the variation of $\Delta\nu_{\rm d}$ in frequency. It is well predicted that $\Delta\nu_{\rm d} \approx \nu^{-\alpha}$ ($\alpha = 4.4$ for the Kolmogorov turbulence or $\alpha = 4.0$ for the Gaussian turbulence). Except scintillation, another prorogation effect called pulse scatter-broadening is often used to estimate α as well (e.g. Bansal et al. 2019; Krishnakumar et al. 2019; Geyer et al. 2017).

In this work, we report our independent measurements of α with LOFAR data set. We obtain the $\Delta\nu_{\rm d}$ from dynamic spectrum with each 10 MHz frequency band, except J0953+0755 of 20 MHz band to reduce the statistical error (Fig.3). Then, based on the measurements of $\Delta\nu_{\rm d}$ that were obtained from a single observation, we are able to get the parameter α without the influence from RISS. The measurements of $\Delta\nu_{\rm d}$ from dynamic spectra, the derived α of 15 nearby pulsars, and $\Delta\nu_{\rm d}$ at other frequencies from previous works (Appendix.A) show in Fig.3. The large uncertainty of $\Delta\nu_{\rm d}$ of J2018+2839 and J2022+5154 is due to low signal to noise ratio that makes a fuzzy 2D ACF. Thus, J2022+5154 does not present in the following discussion.

The α values are mostly coincidence with the prediction from the kolmogorov spectrum or Gaussian spectrum, except J1239+2453 ($\alpha = 3.21 \pm 0.29$) and J2022+2854 ($\alpha = 6.56 \pm 0.24$). For convenient, the red lines that represent the prediction $\alpha = 4.4$ are also presented for this two pulsars in Fig.3. For J2022+2854, kolmogorov assumption gives a better prediction at wider frequency range for long time span. However, it is hardly to determine which α gives a better result for J1239+2453. A low value of α may be due to the associations with HII regions, arms or supernova remnants (Krishnakumar et al. 2019), anisotropic scattering screens (Geyer et al. 2017) or flatter spectra due to the fact that the diffraction scale $s_{\rm d}$ becomes smaller than the inner scale at lower frequencies (e.g. Bansal et al. 2019). For J1239+2453, the $s_{\rm d} \sim 1/(k\theta_{\rm d}) \sim 31000$ km which is larger than the inner scale, where $\theta_{\rm d}$ is the width of the angular scattering given by $(c/\pi D_{\rm p}\Delta\nu_{\rm d})^{0.5} \sim 2.1$ mas in which $D_{\rm p} = 0.85\pm0.06$ kpc (Brisken et al. 2002) and k is the wave number, following Rickett (1990). At least for this observation, a flatter spectra is not the reason that causes the smaller α. We note that anisotropic scattering screens could be the one of reasons of low value of α as the α of most of pulsars with scintillation arc resulting from highly anisotropic scattering screens are slightly smaller than the prediction value from Kolmogorov turbulence although we have moderately large uncertainties. For B2020+28, this large α could because of larger scattering regions involved, which may suggest that the effect of refractive scattering is large and is independent of observing frequency (Goodman & Narayan 1985). This requires further investigation of RISS and is beyond the scope of this work. Our α values for J0032+5434, J2018+2839 and J2219+4754 agree with the values reported in the literature (Krishnakumar et al. 2017; Bansal et al. 2019; Krishnakumar et al. 2019). However, our α measurement of J0826+2637 differs from α values of 1.55±0.40 (Deller et al. 2019) and 2.4±0.1 (Krishnakumar et al. 2019). This could simply due to the different epochs of the used data set since the α exhibits variation over time (Bansal et al. 2019). For other pulsars, we do not notice the α reported based on pulse scattering broadening. Actually, the time delay could be tiny at higher frequencies, causing unresolved pulse broadening. New extension in nançay upgrading LoFAR has great potential on this (Bondonneau et al. 2020).

With α, we are able to predict scintillation bandwidth at other frequencies (see Fig.3 and Appendix A). Those $\Delta\nu_{\rm d}$ from previous works are consistent with our predictions for some pulsars, for example, 0823+26, 0809+74. However, there are some pulsars having significantly divergence, B0834+06 and B1133+16. The $\Delta\nu_{\rm d}$ values from published works are about 100 times than our prediction. The discrepancy partly caused by refractive scintillation. B0834+06 is well-known pulsar with 1D underlying phase-changing screen (Brisken et al. 2010). Stinebring et al. (2019) also identified that one-dimensional(1D), linear brightness function is in good agreement with the B1133+16 at 327, 432, 1450 MHz. This cases of J0837+0610 and B1136+1551 raise a question of if the amplitude of scintillation parameters variation varies with the level of anisotropic scattering screen. Long term scintillation monitoring is sensitive to this question. The finite dynamic spectrum both in frequency and time space could be another reason, in particular at higher observing frequencies. An another explanation could be the different ISM structure in the line of sight, after all, it is possible that the differences might be simply due to the measurements from observations made over separations of years. Overall, our predictions are consistent with the others at Lower observing frequencies, however, inconsistent for higher frequencies. This could partly result from the limited frequency band and observing length at higher frequencies.

3.2. scintillation arc

The interference between the scattered ray at θ and the unscattered ray at the center of the scattering image results in a differential geometric time delay τ and differential Dopple shift $f_{\rm D}$ of each ray, corresponding a single point in the main parabolic of the secondary spectrum with the arc curvature η in the form of:

$$\tau = \eta f_{\rm D}^2, \tag{8}$$

where arc curvature η is

$$\begin{aligned}\eta &= \frac{D_{\rm p} s(1-s)}{2\nu^2}\frac{c}{(\boldsymbol{V_{\rm eff}}\cos\psi)^2} \\ &= 4.629\times10^3\frac{D_{\rm p,kpc}\, s(1-s)}{V_{\rm GHz}^2(\boldsymbol{V_{\rm eff,km}}\cos\psi)^2} \quad ({\rm second/Hz^2})\end{aligned} \tag{9}$$

where ψ is the angular separation between a component of the scattered image and the line-of-sight for anisotropy scattering screen (Coles et al. 2005).

For single pulsars, the effective transverse line-of-sight velocity $\boldsymbol{V_{\rm eff}}$ contain three components: the transverse velocity $\boldsymbol{V_{\rm p}}$, the earth motion $\boldsymbol{V_{\rm E}}$ and the movement of scattering material $\boldsymbol{V_{\rm ISM}}$ with the form of

$$\boldsymbol{V_{\rm eff}} = (1-s)\boldsymbol{V_{\rm p}} + s\boldsymbol{V_{\rm E}} - \boldsymbol{V_{\rm ISM}}(s), \tag{10}$$

In this work, ψ is assumed to 0 and we ignore $\boldsymbol{V_{\rm ISM}}$. Long term scintillation monitoring is sensitive to this two parameters by modeling the annual variation of arc curvature (Main et al. 2020; Reardon et al. 2020), the orbital or annual variations of scintillation velocity (Reardon et al. 2019).

In summary, scintillation arc is a phenomenon with a bunch of applications (see introduction), we only discuss the placement, spatial scale of the scattering screen and the possible potential influence on PTA in this work.

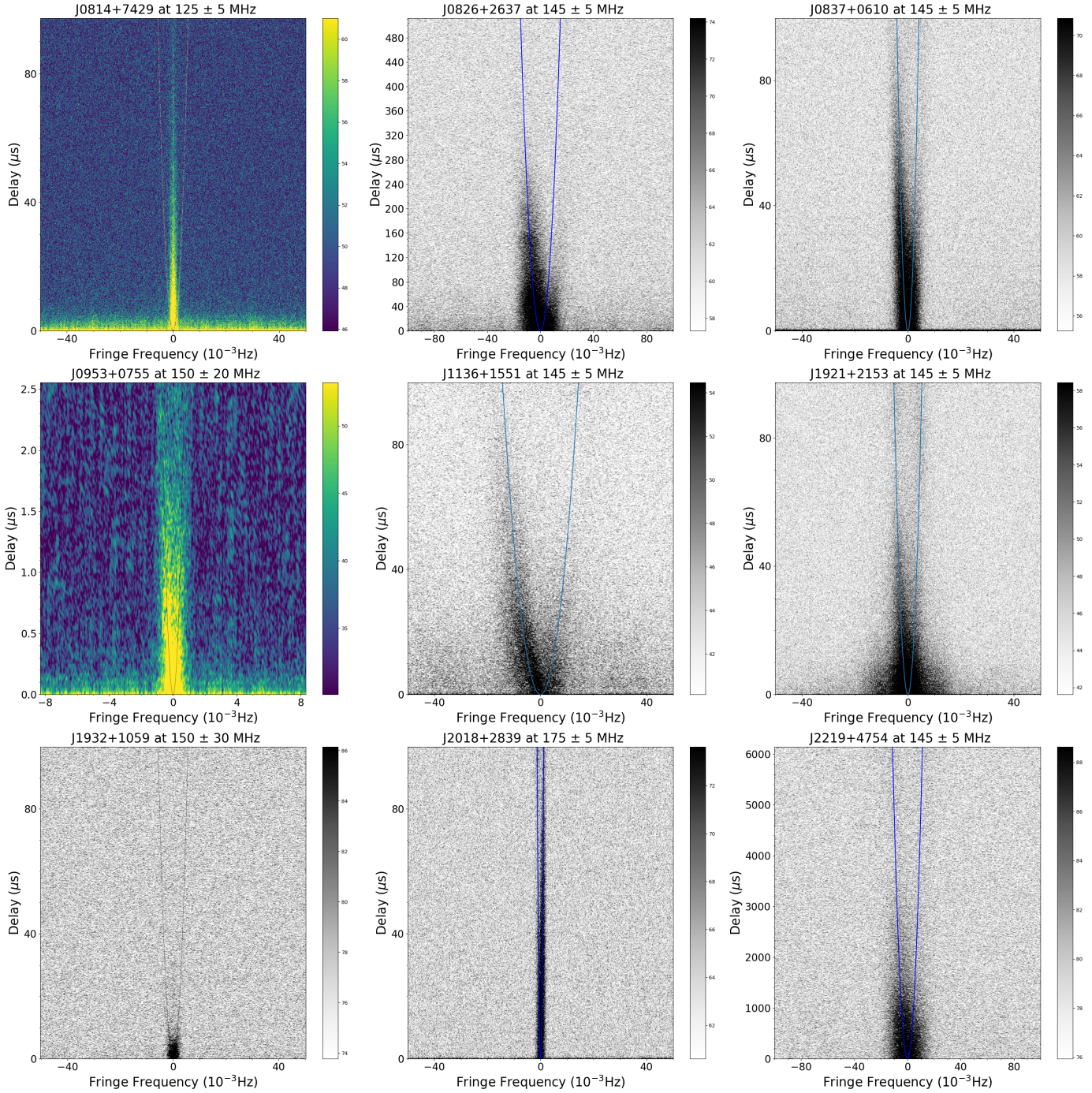

Fig. 4: Scintillation arcs from 8 pulsars with LOFRA. The blue line is a parabola with the measured arc curvature in text.

3.2.1. The distance of the scattering screen

9 slow pulsars can be found with scintillation arc at LOFAR frequency (Fig. 4). Arc curvature is larger at lower frequencies (more close to the Fringe Frequency = 0) and diffuse and thick. This makes the some particular scintillation arc sources are indistinct. Moreover, the asymmetry arcs prove the presence of dispersion, refraction and phase gradient (Coles et al. 2010). The arc curvature (Tab.2) of detected arcs.

J0814+7429 We report that a highly asymmetry arc from this pulsar is first detected. The scattering is distributed at the 350±1pc from the earth which is consistent with 310pc based on weak scintillation (Rickett et al. 2000).

J0826+2637 This pulsar can be observed with four-arcs (Putney & Stinebring 2006) and single-arc (Stinebring et al. 2001) at different epochs. The arc we observed is consistent with the "c" arc reported by (Putney & Stinebring 2006). The screen that dominates the scattering is at 187±15pc.

J0837+0610 Clear arc-let and 1ms isolated feature are well detected though VLBI (Brisken et al. 2010). The location of the screen is located at 460±80pc (Hill et al. 2005) or 420pc(Brisken et al. 2010) or 210pc for the main arc (Smirnova et al. 2020). Our result however show that the scattering screen is located at 326±1pc from the earth.

J0953+0755 Smirnova et al. (2014) suggested that the observed parameters of scintillation effects indicate that two

Table 2: The measured location of scattering screen of 8 pulsars with arc based on the arc curvature

PSRs	MJD	Freq. (MHz)	curvature (s^3)	D_s (pc)	D_p^{ref} kpc	D_s^{ref} (pc)	$L_{s,\|\|}$ (au)
J0814+7429	57872	125±5	2.97±0.01	350±1	0.433±0.008[f]	310pc[a]	0.05
J0826+2637	58820	145±5	2.27±0.27	187^{+13}_{-17}	0.5±0.00[g]	[1-(0.06, 0.25, 0.62, 072)]D[j]	0.19
J0837+0610	58867	145±5	5.81±0.04	326 ±1	0.62±0.06[l]	460±80[d], 420[e], 210[h],	0.22
J0953+0755	57391	150±20	5.09±0.09	233±x	0.262±0.005	4.4–16.4 pc and 26–170 pc [o]	≥0.01
J1136+1551	57122	145±5	0.45± 0.08	113^{+15}_{-11}	0.35±0.02[f]	≥136[i]	0.09
J1921+2153	58356	145±5	3.46±0.33	564±x	0.81[n]	440	≥0.13
J1932+1059	59213	150±30	3.12±0.15	175 ±3	0.331±0.01[f]	200±20[k], 240±30[m]	0.04
J2018+2839	58844	175±5	61.81 ± 4.30	612^{+27}_{-30}(or 290^{+27}_{-35})	0.95±0.09[f]	≤100[m]	≥0.15
J2219+4754	58863	145 ±5	48.41 +- 8.11	-	-	-	-

[ref] References: ([a]) Rickett et al. 2000, ([c]) Stinebring et al. 2001, ([d]) Hill et al. 2005, ([e]), Brisken et al. 2010, ([f])Brisken et al. 2002, ([g])Deller et al. 2019, ([h])Smirnova et al. 2020, ([i])Stinebring et al. 2019, ([j])Putney & Stinebring 2006, ([k])Yao et al. 2020, ([l])Liu et al. 2016, ([m])Fadeev et al. 2018, ([n])Yao et al. 2017, ([o])Smirnova et al. 2014.

plasma layers lie along the line of sight to the pulsar, at distances of 4.4–16.4 pc and 26–170 pc. The closest pulsar in our scintillating pulsar list shows an asymmetry arc (left side stronger). The screen that dominate the scattering is at 233pc from the observer which is 30 pc from the pulsar. This pulsar is surround by a nebula (Ruan et al. 2020; Manning & Willmore 1994), however, the nebula is unlikely to extend this distance.

J1136+1551 This pulsar is also a 4-arcs source (Putney & Stinebring 2006) and a one-dimensional (1D), linear brightness function is in good agreement with the observed arcs at different observing frequencies with the placement of ≥136pc from the earth (Stinebring et al. 2019). which is consistent with our measurement of d_s = 113±15pc.

J1921+2153 Shishov et al. (2017) argue that diffractive scintillation from inhomogeneities in a layer of turbulent plasma at a distance 440 pc from the observer or homogeneously distributed scattering material to the pulsar. The observed single arc with LOFAR indicates that the scattering is dominated by a thin screen with a placement of 258±4 pc from the earth.

J1932+1059 This pulsar can be observed with three-arcs (Putney & Stinebring 2006) and single-arc (Fadeev et al. 2018; Yao et al. 2020) at different epochs. The placement of the screen is at 200±20pc (Yao et al. 2020) and 240±30pc (Fadeev et al. 2018), which is consistent with our result 175±3 pc. Similar to J0953+0755, this pulsar is also surround by a nebula (Hui & Becker 2008). However, the most scattering of pulsar signal is not contributed by the nebula. Partly reason could be the small electronic density of nebula. Hill et al. (2005) measured that the electronic density of the screen regrading the scintillating arc from B0834+06 can be up to 2000 cm^{-3} which makes that the scattering from nebula is ignorable.

J2018+2839 Fadeev et al. (2018) proposed that the scattering layer may be located significantly closer to the observer than 100 pc. However, we found that the scattering lay is almost contributed at 612±30 or 290±30 pc (There are two suitable solutions for a given arc curvature of J2018+2839).

J2219+4754 This is the first pulsar with detection of frequency-dependent, time-variable dispersion measures (Donner et al. 2019). These authors also proposed that the spatial scal of the screen is up to 10s of AUs. The arc curvature of this pulsar at 145 MHz is 48.41±8.11 s^{-3}. The fraction distance of the screen is a complex number based on Eq.8 if we ignore the IISM velocity. Michilli et al. (2018) proposed that the distance of the IISM structure from Earth is 1.1±0.2 kpc, approximately half the pulsar distance. If s = 0.5, the arc curvature should be ∼4 s^3. Then, at the Doppler shift -40 (10^{-3} Hz), the time delay at second spectrum is 4×40^2 = 6400 us, which is not the case as we show in Fig. 4. If we take the IISM velocity into consideration, if the scattering screen is at half the pulsar distance, the IISM velocity must be comparable to 200 km/s. Typically, the IISM velocity is ≤10 km/s. On the contrary, the velocity of supernova can be up to 4000 km/s (SN1987A). However, there is no associations with H II regions, arms or supernova remnants. Thus, we prefer a very nearby screen that dominates the scintillation effect.

3.2.2. The spatial scale of the screen

In fact, the f_ν-axis is proportional to the time delay relative to an undeflected ray. Now, we discuss the angular extent of the scattering material parallel to the direction of the pulsar velocity given by

$$\theta = \sqrt{\frac{2 f_\nu sc}{D_p(1-s)}} \tag{11}$$

then, corresponding to a linear extent of

$$L_s = 2\tan(\theta) D_p(1-s) \tag{12}$$

corresponds the size of scattering screen (see Fig.2). The spatial scales of the screen are both AU scale with the time delay detected by the eyes. In particular, the size of the present scattering structure of J0834+06 is 0.2 AU (Hill et al. 2005) or <0.5 AU (Brisken et al. 2010) consisting our measurement of 0.22 AU. For J0953+0755, J1921+2153 and J2018+2839, the time delay is beyond the nyquist frequency. Thus, the actual scale should be at least larger than what we can detect with current frequency resolution in Tab.1.

3.2.3. Impart on Pulsar Timing Array

The folded pulse profiles could be cross-correlated with the template profile in order to archive the phase of the observation and archive pulse-arrival times (TOA). For more detail about PTA, the potential reader is recommended to Verbiest et al. (2021). In particular, the time-delay of J2219+4754 (P0 ∼ 0.538s) is extended on the left to delays of 3 ms which is ∼6 phase bin if

nbin = 1024. However, the time-delay resulting from inhomogeneous media is time-variable (Hemberger & Stinebring 2008; Main et al. 2020). This leds timing residuals.

The time delay can be up to 3 us for very close pulsar J1136+1551 (DM = 4.84) (Stinebring et al. 2019) and B1929+10 (DM= 3.18) (Yao et al. 2020) at 1.4 GHz. Current PTAs for detecting low-frequency gravitational waves rely on millisecond pulsars (MSP, DM < 50, mostly, Verbiest et al. 2016), their time delay could be relative larger than 3 us. For a MSP with period of 3 ms, if the phase bin is 1024, each phase bin is about 3us. Thus, the pulse shape may be change resulting from scintillation. The variation of time delay could raise timing noise.

3.3. Pulse nulling

We have identified two pulsar (J0034-0721 and J2022+5154) with pulse nulling and scintillation effect simultaneously (Fig.1 and Fig.5). This two pulsars are both confirmed with nulling state (Huguenin et al. 1970; Ritchings 1976). We note that this is the first time that pulse nulling is reported at such low observing frequency. The nulling fraction of J2022+5154 is 1.4 % at 610 MHz (Gajjar et al. 2012). However, its nulling fraction seems >50% at LOFAR by eyes. The scintillation time-scale of J0034-0721 and J2022+5154 are 2961±592 s at 327 MHz (Bhat et al. 1998) and 36±3 min at 1.54 GHz (Wang et al. 2005), respectively. Their $\tau_{\rm d}$ at our frequency should be ∼20 min and ∼2.2 min at 150 MHz, respectively, using the $\nu^{1.2}$scaling form. We note that the proper motion of these two pulsars are 74.28 km/s and 107.81 km/s (obtained from "psrcat"), respectively, so the scintillation time-scale could be modulated by earth motion.

If the pulse nulling is presence, the intensity of ACF in time lag is weak than the truth intensity at some points of time lag axis, which could cause untrustworthy measurements of scintillation time-scale. In contrast, the influence coming from pulse nulling on scintillation bandwidth may be ignorable.

4. Conclusion and future works

We have reported the first census of 15 scintillating pulsars (DM < 50) with LOFAR at 120-180 MHz frequency band. The frequency dependencies of $\Delta\nu_d$ imply that the turbulence feature of the interstellar medium deviates from the Kolmogorov turbulence at different level. Highly asymmetry arcs from 9 pulsar have been detected, which is used to estimate the fraction distance of the phase changing screen. In particularly, the independent measurement of frequency scaling factor of $\Delta\nu_d$ without the effect coming from refractive scintillation and the extraordinary record of time delay of 3 ms at secondary spectrum of J2217+4754 constantly prove the possibility of further pulsar scintillation studies with LOFAR.

Long term scintillation monitoring of our pulsars is being processed with LOFAR. The annual variations of scintillation time-scale and arc curvature resulting from earth motion are confirmed. The correlation between scintillation and DM is detected as well. At least two papers regrading scintillation with LOFAR are coming.

Acknowledgements. Five Germany stations and one French stations of the International LOFAR Telescope (ILT), constructed by ASTRON, are owned and operated by partners: the Effelsberg (DE601) station funded by the Max-Planck-Gesellschaft; the Tautenburg (DE603) station funded by the State of Thuringia and supported by the European Union (EFRE) and the Federal Ministry of Education and Research (BMBF) Verbundforschung project D-LOFAR I (grant number 05A08ST1); the Potsdam (DE605) station supported by the Leibniz-Institut for Astrophysik, Potsdam, the Norderstedt (DE609) funded by the BMBF (grant 05A11LJ1) and the states of Nordrhein-Westfalia and Hamburg, and Nançay (FR606). The observations of the German LOFAR stations were carried out in the stand-alone GLOW mode which is technically operated and supported by the Max-Planck-Institut für Radioastronomie, the Forschungszentrum Jülich, Bielefeld University, by BMBF Verbundforschung project D-LOFAR III (grant number 05A14PBA) and by the states of Nordrhein-Westfalen and Hamburg. The observations during this project were made during station-owners time as well as during ILT time allocated under project codes LC0_014, LC1_048, LC2_011, LC3_029, LC4_025 and LT5_001. This project also benefited greatly from the ILT Core observations that were included in the Michilli et al. (2018) paper and which guided some of the analysis and interpretation in this paper. Those observations were carried out under ILT time allocation codes LC0_011, LC1_027, LC2_010, LT3_001, LC4_004 and LT5_003.

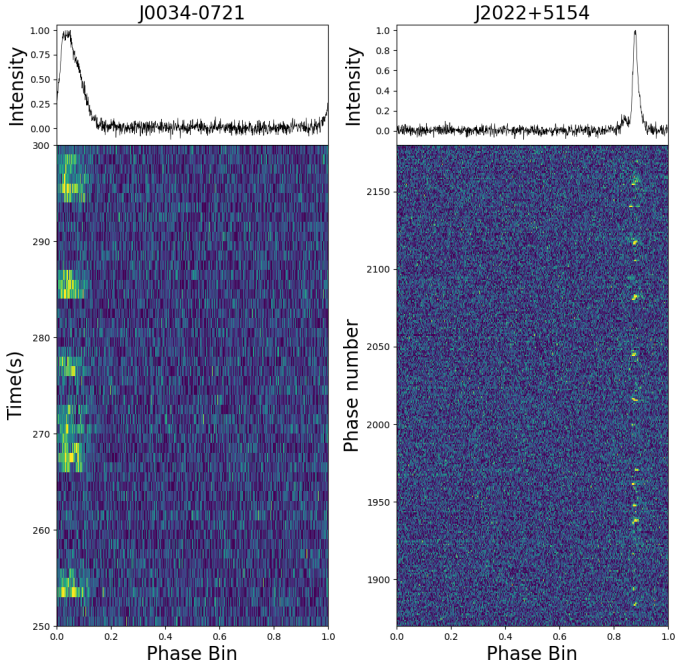

Fig. 5: Left: Right: Top: The pulse profile averaged over the whole data span is shown. Bottom: 30 min long single pulse sequence for PSR J2022+5154, in which increasing yellowness represents higher intensity. Pulse nulling is observed clearly.

References

Armstrong, J. W. & Rickett, B. J. 1981, MNRAS, 194, 623
Armstrong, J. W., Rickett, B. J., & Spangler, S. R. 1995, ApJ, 443, 209
Backer, D. C. 1974, ApJ, 190, 667
Balasubramanian, V. & Krishnamohan, S. 1985, Journal of Astrophysics and Astronomy, 6, 35
Bansal, K., Taylor, G. B., Stovall, K., & Dowell, J. 2019, ApJ, 875, 146
Bell, M. E., Murphy, T., Johnston, S., et al. 2016, MNRAS, 461, 908
Bhat, N. D. R., Gupta, Y., & Rao, A. P. 1998, ApJ, 500, 262
Bhat, N. D. R., Gupta, Y., & Rao, A. P. 1999a, ApJ, 514, 249
Bhat, N. D. R., Ord, S. M., Tremblay, S. E., McSweeney, S. J., & Tingay, S. J. 2016, ApJ, 818, 86
Bhat, N. D. R., Rao, A. P., & Gupta, Y. 1999b, ApJS, 121, 483
Bondonneau, L., Grießmeier, J. M., Theureau, G., et al. 2020, arXiv e-prints, arXiv:2009.02076
Brisken, W. F., Benson, J. M., Goss, W. M., & Thorsett, S. E. 2002, ApJ, 571, 906
Brisken, W. F., Macquart, J. P., Gao, J. J., et al. 2010, ApJ, 708, 232
Coles, W. A., McLaughlin, M. A., Rickett, B. J., Lyne, A. G., & Bhat, N. D. R. 2005, ApJ, 623, 392
Coles, W. A., Rickett, B. J., Gao, J. J., Hobbs, G., & Verbiest, J. P. W. 2010, ApJ, 717, 1206
Cordes, J. M. 1986, ApJ, 311, 183
Cordes, J. M. & Rickett, B. J. 1998, ApJ, 507, 846

Cordes, J. M., Rickett, B. J., Stinebring, D. R., & Coles, W. A. 2006, ApJ, 637, 346
Cordes, J. M., Weisberg, J. M., & Boriakoff, V. 1985, ApJ, 288, 221
Daszuta, M., Lewandowski, W., & Kijak, J. 2013, MNRAS, 436, 2492
Deller, A. T., Goss, W. M., Brisken, W. F., et al. 2019, ApJ, 875, 100
Donner, J. Y., Verbiest, J. P. W., Tiburzi, C., et al. 2019, A&A, 624, A22
Fadeev, E. N., Andrianov, A. S., Burgin, M. S., et al. 2018, MNRAS, 480, 4199
Gajjar, V., Joshi, B. C., & Kramer, M. 2012, MNRAS, 424, 1197
Geyer, M., Karastergiou, A., Kondratiev, V. I., et al. 2017, MNRAS, 470, 2659
Goodman, J. & Narayan, R. 1985, MNRAS, 214, 519
Gupta, Y. 1995, ApJ, 451, 717
Gupta, Y., Rickett, B. J., & Lyne, A. G. 1994, MNRAS, 269, 1035
Hall, A. N. 1980, MNRAS, 191, 739
Hemberger, D. A. & Stinebring, D. R. 2008, ApJ, 674, L37
Hill, A. S., Stinebring, D. R., Asplund, C. T., et al. 2005, ApJ, 619, L171
Hotan, A. W., van Straten, W., & Manchester, R. N. 2004, PASA, 21, 302
Huguenin, G. R., Taylor, J. H., & Troland, T. H. 1970, ApJ, 162, 727
Hui, C. Y. & Becker, W. 2008, A&A, 486, 485
Johnston, S., Nicastro, L., & Koribalski, B. 1998, MNRAS, 297, 108
Kondratiev, V. I., Popov, M. V., Soglasnov, V. A., & Kostyuk, S. V. 2001, Ap&SS, 278, 43
Krishnakumar, M. A., Joshi, B. C., & Manoharan, P. K. 2017, ApJ, 846, 104
Krishnakumar, M. A., Maan, Y., Joshi, B. C., & Manoharan, P. K. 2019, ApJ, 878, 130
Lazarus, P., Karuppusamy, R., Graikou, E., et al. 2016, MNRAS, 458, 868
Levin, L., McLaughlin, M. A., Jones, G., et al. 2016, ApJ, 818, 166
Liu, S., Pen, U.-L., Macquart, J. P., Brisken, W., & Deller, A. 2016, MNRAS, 458, 1289
Main, R. A., Sanidas, S. A., Antoniadis, J., et al. 2020, MNRAS, 499, 1468
Malofeev, V. M., Smirnova, T. V., Soin, A. G., & Shapovalova, N. V. 1995, Astronomy Letters, 21, 619
Manning, R. A. & Willmore, A. P. 1994, MNRAS, 266, 635
Michilli, D., Hessels, J. W. T., Donner, J. Y., et al. 2018, MNRAS, 476, 2704
Narayan, R. 1992, Philosophical Transactions of the Royal Society of London Series A, 341, 151
Niu, H. B., Esamdin, A., & Wang, N. 2013, Ap&SS, 347, 327
Pen, U.-L. & Levin, Y. 2014, MNRAS, 442, 3338
Phillips, J. A. & Clegg, A. W. 1992, Nature, 360, 137
Putney, M. L. & Stinebring, D. R. 2006, Chinese Journal of Astronomy and Astrophysics Supplement, 6, 233
Reardon, D. J., Coles, W. A., Bailes, M., et al. 2020, ApJ, 904, 104
Reardon, D. J., Coles, W. A., Hobbs, G., et al. 2019, MNRAS, 485, 4389
Rickett, B., Johnston, S., Tomlinson, T., & Reynolds, J. 2009, MNRAS, 395, 1391
Rickett, B. J. 1970, MNRAS, 150, 67
Rickett, B. J. 1977, ARA&A, 15, 479
Rickett, B. J. 1990, ARA&A, 28, 561
Rickett, B. J., Coles, W. A., & Markkanen, J. 2000, ApJ, 533, 304
Rickett, B. J., Coles, W. A., Nava, C. F., et al. 2014, ApJ, 787, 161
Ritchings, R. T. 1976, MNRAS, 176, 249
Roberts, J. A. & Ables, J. G. 1982, MNRAS, 201, 1119
Ruan, D., Taylor, G. B., Dowell, J., et al. 2020, MNRAS, 495, 2125
Safutdinov, E. R., Popov, M. V., Gupta, Y., Mitra, D., & Kumar, U. 2017, Astronomy Reports, 61, 406
Shishov, V. I., Smirnova, T. V., Gwinn, C. R., et al. 2017, MNRAS, 468, 3709
Smirnova, T. V. & Shishov, V. I. 2008, Astronomy Reports, 52, 736
Smirnova, T. V., Shishov, V. I., Andrianov, A. S., et al. 2020, MNRAS, 496, 5149
Smirnova, T. V., Shishov, V. I., Popov, M. V., et al. 2014, ApJ, 786, 115
Smith, F. G. & Wright, N. C. 1985, MNRAS, 214, 97
Spangler, S. R. & Gwinn, C. R. 1990, ApJ, 353, L29
Stinebring, D. R., Faison, M. D., & McKinnon, M. M. 1996, ApJ, 460, 460
Stinebring, D. R., McLaughlin, M. A., Cordes, J. M., et al. 2001, ApJ, 549, L97
Stinebring, D. R., Rickett, B. J., & Koch Ocker, S. 2019, ApJ, 870, 82
Trang, F. S. & Rickett, B. J. 2007, ApJ, 661, 1064
van Haarlem, M. P., Wise, M. W., Gunst, A. W., et al. 2013, A&A, 556, A2
van Straten, W. & Bailes, M. 2011, PASA, 28, 1
Verbiest, J. P. W., Lentati, L., Hobbs, G., et al. 2016, MNRAS, 458, 1267
Verbiest, J. P. W., Oslowski, S., & Burke-Spolaor, S. 2021, arXiv e-prints, arXiv:2101.10081
Verbiest, J. P. W. & Shaifullah, G. M. 2018, Classical and Quantum Gravity, 35, 133001
Walker, M. A., Koopmans, L. V. E., Stinebring, D. R., & van Straten, W. 2008, MNRAS, 388, 1214
Walker, M. A., Melrose, D. B., Stinebring, D. R., & Zhang, C. M. 2004, MNRAS, 354, 43
Wang, N., Manchester, R. N., Johnston, S., et al. 2005, MNRAS, 358, 270
Wang, N., Yan, Z., Manchester, R. N., & Wang, H. X. 2008, MNRAS, 385, 1393
Wang, P. F., Han, J. L., Han, L., et al. 2018, A&A, 618, A186
Wolszczan, A. 1977, Acta Astron., 27, 127
Xu, S. & Zhang, B. 2017, ApJ, 835, 2
Yao, J., Zhu, W., Manchester, R. N., et al. 2021, arXiv e-prints, arXiv:2103.01839
Yao, J. M., Manchester, R. N., & Wang, N. 2017, ApJ, 835, 29
Yao, J.-M., Zhu, W.-W., Wang, P., et al. 2020, Research in Astronomy and Astrophysics, 20, 076

Appendix A: Scintillation Bandwidth from Literature

PSRs J	Freq. (MHz)	$\Delta\nu_d$ (MHz)	Ref.
0034-0721	408	4	7
	436	3.80	6
	660	7.55	6
	327	1.039±0.208	24
0332+5434	327	0.130 ± 0.004	1
	408	0.8	5
	610	4.0	5
	408	0.03	7
	1000	3.89	8
	408	0.047	9
	1540	14±1	12
	1540	9.2±2.2	15
	2250	17±2	13
	2250	20±2	13
	2250	67±14	13
	610	349	20
	327	60	21
	610	220	21
	610	130	21
	1420	5930	21
	327	0.165±0.013	24
	340	0.036	25
	408	0.088	25
	102.5	0.243	26
0814+7429	41	0.002 ± 0.0006	3
	62.43	0.007 ± 0.003	3
	88.57	0.020 ± 0.010	3
	111.87	0.045 ± 0.005	3
	151	1.2	5
	408	≥ 30	5
	408	4	7
	1000	85.114	8
	51.5	0.0039±0.0007	18
	81.5	0.023±0.001	18
0826+2637	327	0.244 ± 0.015	1
	327	0.287 ± 0.018	1
	327	0.250 ± 0.008	1
	430	0.396	2
	430	0.215	2
	326.5	0.058	23
	408	0.5	7
	1000	33.113	8
	408	0.189	9
	102.7	0.0014±0.0003	10
	1540	82±5	12
	1700	81±3	14
	327	0.293±0.041	24
0837+0610	327	0.419 ± 0.014	1
	327	0.493 ± 0.022	1
	327	0.369 ± 0.011	1
	327	0.353 ± 0.008	1
	327	0.616 ± 0.017	1
	408	5.5	5
	335	0.350	4
	410	0.280	4
	410	1.450	4
	430	0.050	2

Continued on next column

Continued from previous column

PSRs J	Freq. (MHz)	$\Delta\nu_d$ (MHz)	Ref.
	430	0.406	2
	430	0.223	2
	430	0.243	2
	430	0.151	2
	430	0.136	2
	430	0.396	2
	326.5	0.495	23
	408	1.6	7
	1000	25.704	8
	408	1.260	9
	102.7	2.3±0.2	10
	324	0.004±0.0005	19
	324	0.350±0.020	19
	324	0.210±0.010	19
	324	0.185±0.010	19
	324	0.280±0.015	19
	324	0.235±0.020	19
	327	0.454±0.027	24
0953+0755	41	0.0015 ± 0.0004	3
	62.43	0.025 ± 0.010	3
	88.57	0.100 ± 0.040	3
	111.87	0.220 ± 0.060	3
	408	≥ 20	5
	436	2.00	6
	320	0.792	2
	320	1.188	2
	430	1.089	2
	1000	162.181	8
	47	0.028 ± 0.002	17
	51	0.049 ± 0.007	17
	51	0.031 ± 0.004	17
	51	0.019 ± 0.001	17
	154	4.1	22
	327	≥9	24
	340	≥1.44	25
	408	≥2.65	25
	450	≥1.75	25
1136+1551	327	0.434 ± 0.018	1
	327	0.838 ± 0.021	1
	327	1.399 ± 0.033	1
	408	≥ 10	5
	430	0.990	2
	430	0.743	2
	430	0.782	2
	430	1.155	2
	326.5	0.710	23
	408	1.3	7
	1000	60.260	8
	102.7	0.0082±0.0006	10
	1540	161.6±27.7	11
	1540	149.2±20.1	11
	1540	134.2±11.4	11
	327	0.816±0.057	24
	340	0.590	25
	408	≥0.97	25
	450	≥1.52	25
1239+2453	327	1.146 ± 0.060	1
	430	0.842	2

Continued on next column

Continued from previous column

PSRs J	Freq. (MHz)	$\Delta\nu_d$ (MHz)	Ref.
	430	0.693	2
	326.5	0.595	23
	408	≥4	7
	1000	61.660	8
	102.7	0.0086±0.0014	10
	1540	154.2±18.4	11
	1540	156.5±24.6	11
	1540	127.0±21.9	11
	327	1.828±0.128	24
	340	≥0.67	25
	408	≥0.99	25
1607-0032	327	0.376 ± 0.015	1
	335	0.020	4
	410	0.035	4
	410	0.050	4
	630	0.670	4
	320	0.376	2
	320	0.248	2
	430	1.089	2
	326.5	0.165	23
	408	≥4	7
	1000	51.286	8
	327	0.378±0.019	24
1921+2153	324	0.33	16
	327	0.295 ± 0.017	1
	327	0.269 ± 0.009	1
	327	0.547 ± 0.011	1
	408	3	5
	335	0.730	4
	410	2.400	4
	320	0.054	2
	320	0.020	2
	320	0.0074	2
	320	0.025	2
	320	0.019	2
	430	0.347	2
	430	0.099	2
	430	0.129	2
	430	0.105	2
	430	0.149	2
	430	0.119	2
	326.5	0.330	23
	408	0.9	7
	1000	23.988	8
	102.7	0.0055±0.0007	10
	327	0.285±0.014	24
	102.5	8.6	26
1932+1059	327	1.199 ± 0.083	1
	335	1.600	4
	410	5.700	4
	410	1.000	4
	320	1.190	2
	320	0.891	2
	320	0.743	2
	320	0.614	2
	408	2.2	7
	1000	138.038	8
	1540	268±24	12

Continued on next column

Continued from previous column

PSRs J	Freq. (MHz)	$\Delta\nu_d$ (MHz)	Ref.
	327	60	21
	327	1.293±0.024	24
2018+2839	327	0.201 ± 0.008	1
	430	0.140	2
	430	0.149	2
	430	0.151	2
	430	0.094	2
	430	0.129	2
	430	0.104	2
	430	0.094	2
	326.5	0.132	6
	408	0.3	7
	1000	6.310	8
	408	0.092	9
	102.7	0.0016±0.0002	10
	610	0.63	21
	327	0.206±0.012	24
2022+2854	327	0.199 ± 0.005	1
	320	0.064	2
	430	0.129	2
	430	0.183	2
	430	0.148	2
	430	0.158	2
	430	0.178	2
	326.5	0.396	23
	408	0.6	7
	1000	13.490	8
	1540	70±5	12
	327	0.270±0.022	24
	408	0.56	25
	450	≥0.83	25
2022+5154	408	0.4	7
	1000	2.291	8
	1540	52±3	12
	610	3.41	21
	610	0.81	21
2219+4754	408	0.056	25
	1000	2.29	8

Concluded

[ref] References: (1) Bhat et al. 1999b, (2) Cordes et al. 1985, (3) Smirnova & Shishov 2008, (4) Roberts & Ables 1982, (5) Rickett 1970, (6) Johnston et al. 1998, (7) Smith & Wright 1985, (8) Cordes 1986, (9) Gupta et al. 1994, (10) Malofeev et al. 1995, (11) Niu et al. 2013, (12) Wang et al. 2005, (13) Wang et al. 2018, (14) Daszuta et al. 2013, (15) Wang et al. 2008, (16) Shishov et al. 2017, (17) Phillips & Clegg 1992, (18) Bondonneau et al. 2020, (19) Smirnova et al. 2020, (20) Stinebring et al. 1996, (21) Safutdinov et al. 2017, (22) Bell et al. 2016, (23) Balasubramanian & Krishnamohan 1985, (24) Bhat et al. 1998, (25) Armstrong & Rickett 1981, (26) Kondratiev et al. 2001